Applied Surface Science 635 (2023) 157709

Contents lists available at ScienceDirect

Applied Surface Science

journal homepage: www.elsevier.com/locate/apsusc

Full Length Article

Significant texture and wear resistance improvement of TiN coatings using pulsed DC magnetron sputtering

N.A. Richter [a,*], B. Yang [a], J.P. Barnard [a], T. Niu [a], X. Sheng [a], D. Shaw [c], M. Watanabe [c], G. Rane [d], U. Krause [d], P. Dürrenfeld [d], H. Wang [a,b], X. Zhang [a,*]

[a] School of Materials Engineering, Purdue University, West Lafayette, IN 47907, USA
[b] School of Electrical and Computer Engineering, Purdue University, West Lafayette, IN 47907, USA
[c] Advanced Energy Industries, Inc., Fort Collins, CO 80525, USA
[d] Advanced Energy Industries GmbH, D-72555 Metzingen, Germany

ARTICLE INFO

Keywords:
Titanium nitride
Pulse DC magnetron sputtering
Transmission electron microscopy
Nanoscratch testing

ABSTRACT

Titanium nitride (TiN) coatings fabricated through reactive sputtering feature a suite of parameters capable of altering the microstructure and properties. Here, we explore the influence of bipolar pulsed direct current (DC) magnetron sputtering on microstructure evolution of TiN coating, in comparison to conventional DC sputtering. The implementation of a pulsed DC voltage profile promotes a drastic texture change from randomly oriented polycrystals to (1 1 1) textured TiN coatings across the full range of pulse frequencies on various Si substrates, including amorphous SiO_2. Additionally, higher pulse frequencies promote significant grain size reduction, accompanied with corresponding increases in hardness and wear resistance. The potential mechanism for this microstructural and texture evolution is also explored.

1. Introduction

Fatigue and wear account for a large percentage of industrial component failure and losses each year and significant effort is taken to reduce the tribological breakdown of materials [1,2]. A means of mitigating this deficiency is through the use of hard protective coatings, typically fabricated using either chemical vapor deposition (CVD) or physical vapor deposition (PVD) [3–9]. Titanium nitride (TiN) is extensively used as a protective coating due to its superior strength [10–12], low coefficient of friction (COF) [12,13] and chemical stability [14] combined with its distinct golden color [15]. The tribological response of TiN is highly relevant to a variety of industrial applications as friction and wear are commonly linked to component failure [1,16,17]. Datta et al. [18] identified a four orders of magnitude wear rate reduction in Ti6Al4V alloys coated with TiN prepared using cathodic arc deposition. Additionally, Kelly et al. demonstrated that Ti based coatings fabricated using unbalanced pulsed DC magnetron sputtering exhibited significantly reduced COFs than their conventional DC counterparts [13,19]. Nanoscratch testing is a technique enabling the exploration of the tribological properties of thin coatings to assess wear properties and film adhesion [20,21]. The scratch speed, loading mode (continuous or ramping), indenter geometry and penetration depth are controllable during testing and directly impact the test results [20–23]. Previous literature has demonstrated nanoscratch test results correlate strongly with various wear test methods, validating its use to assess the tribological response of nitride coatings [24–27].

TiN is frequently fabricated by reactive sputtering, where the sputtered target atoms react with a "reactive" gas (nitrogen) to produce the nitride films [28,29]. The relationship between reactive sputter process conditions and resulting nitride film structure have been extensively studied due to their strong influence on resulting properties [30–32], for both functional [33,34] and structural applications [32,35]. There are a plenitude of process parameters that directly alter film structure and coating properties, including reactive gas partial pressure [33,36,37], overall gas pressure [31,38], substrate temperature or bias [37,39–41], applied power [42], distance between the substrate and target [38,43], and film thickness [44–46]. There has been extensive debate over the origins of a preferred orientation during film growth, and Kajikawa et al. provided a detailed review of this topic [31]. Their work identified that surface diffusion, grain growth and sticking probability are all competing processes that promote a specific film texture [31], and all of these processes can be manipulated by altering plasma conditions

* Corresponding authors.
E-mail addresses: richtern@purdue.edu (N.A. Richter), xzhang98@purdue.edu (X. Zhang).

https://doi.org/10.1016/j.apsusc.2023.157709
Received 20 February 2023; Received in revised form 24 May 2023; Accepted 3 June 2023
Available online 5 June 2023

during deposition.

In reactive sputtering, reactive gas ions react with both the sputtered target atoms as well as the metallic target surface itself [47–49], leading to charge buildup that degrades deposition rate and reduces film quality due to arc events [45,50]. A popular innovation to circumvent this issue is pulsed direct current (DC) magnetron sputtering, which has become widely used to fabricate high quality stochiometric compound films. Pulsed DC applies a pulse voltage to the target material and can be pulsed using either a unipolar (between a positive voltage and 0 V) or bipolar (between a positive and negative voltage) profile. The bipolar polarity reversal attracts free electrons active in the plasma back to the target surface, wiping out surface charge buildup during reactive sputtering [48,51,52]. This suppresses arc events and decreases the growth rate of insulating and dielectric compounds [52–54]. Kelly et al. presented a significant improvement in film quality and mechanical properties of titania coatings deposited using pulsed DC reactive sputtering [13].

Similarly, it has been demonstrated that introducing a pulsed voltage profile during reactive sputtering of TiN can alter the resulting grain morphology, and typically restricts grain size [55]. Yeh et al. [56] demonstrated that TiN coatings deposited using pulsed DC exhibited higher hardness and improved resistivity compared with its conventional DC counterparts. Compared with conventional DC sputtering, pulsed DC sputtering increases both the ratio of fluxes of bombarding ions and the bombarding ion energies, leading to denser films with reduced grain size and higher degrees of compressive residual stress [13,57–59]. High power impulse magnetron sputtering (HiPIMS) is another pulsed DC reactive sputtering methodology where high power densities are achieved promoting denser films and refined microstructures leading to improved performance [60–62]. Additionally, gas injection magnetron sputtering (GIMS) pulses the plasma forming gas rapidly to avoid insulating compound buildup on the target surface and has demonstrated success in depositing TiN and TiO_2 coatings [63,64]. In spite of these studies on TiN coatings, the influence of pulse frequencies during bipolar pulsed DC depositions on the texture, microstructure and properties of TiN coatings remain unclear.

This work probes the influence of using a pulsed DC power supply on the resulting microstructure, texture and wear properties of TiN coatings. Through a systematic probing of various pulse frequencies, it is established that the introduction of a pulsed voltage profile dramatically influences the film texture. Detailed microscopy uncovers the microstructural refinement at higher pulse frequencies, and nanoindentation and nanoscratch testing demonstrate an improvement in wear properties. This study provides a novel framework for tailoring TiN film texture and bolstering film properties by using bipolar pulsed DC sputtering.

2. Experimental methods

Titanium nitride (TiN) coatings were deposited using an AJA ATC-2200-UHV magnetron sputtering system on hydrofluoric acid (HF) etched Si(1 0 0) substrates via reactive sputtering. The coating process was conducted using a mixture of Ar (sputtering) and N_2 (reactive) gases, the ratio of which was controlled using independent mass flow controllers. An overall gas pressure was maintained at 3.7 mTorr using an adjustable gate valve in front of a turbomolecular pump, and the flow rates were 29 sscm Ar and 0.8 sscm N_2. A high purity Ti (99.99%) target 76.5 mm in diameter and 6 mm thick was used in a vacuum chamber evacuated to 8×10^{-9} torr with a substrate-to-target distance of 150 mm. Circular, unbalanced magnetrons were used in the AJA ATC-2200-UHV magnetron sputter system with a deposition rate of 0.1 nm/s. A conventional direct current (DC) power supply and an Advanced Energy Pinnacle^{TM} Plus + pulsed DC power supply (supplied by Advanced Energy) were used to compare the coating property variation with different power supply method. To maintain a direct comparison between the two power supplies, a power of 300 W was applied during every deposition, and a substrate temperature of 200 °C and a substrate bias of −20 V were used for every deposition The pulse frequency was then varied over a range of 50 kHz to 300 kHz. Additionally, the pulsed DC power supply operates in an asymmetric bipolar mode where the voltage is reversed to ~10% of the negative pulse-on voltage while pulsed. The film thickness was controlled to ~700 nm by determining the deposition rate using a built-in quartz crystal rate monitor.

A Panalytical Empyrean X′pert PRO MRD diffractometer operated at 40 kV using Cu Kα1 X-rays was used to perform X-ray diffraction (XRD) θ–2θ scans to evaluate the overall texture and structure. Transmission electron microscopy (TEM) samples were prepared by mechanical grinding, dimpling, and low-energy ion milling. The microstructure and composition were examined using an Thermo Fischer-FEI Talos 200X analytical microscope operated at 200 kV with a Fischione high-angle annular dark field (HAADF) detector and super X energy-dispersive X-ray spectroscopy (EDS) detector. The line intercept method was utilized with a minimum of 150 grains measured to ensure statistical significance. These grains were measured from HAADF scanning transmission electron microscopy (STEM) images. Crystallographic orientation mapping and grain boundary misorientation measurements were made using Nanomegas ASTAR^{TM} with a camera length of 205 mm, a precession angle of 0.6°, and a step size of 8 nm using the same TEM microscope.

Hardness and elastic modulus were measured using a Bruker TI Premier nanoindenter operated using displacement control mode. A high load transducer capable of applying 1 N was used for nanoindentation. 25 indents were made per sample and the indentation depth was kept below 15% of the film thickness (~150 nm) to prevent incorporating substrate effects. Nanoscratch tests were conducted using a diamond conical tip and the same high load transducer mentioned previously on the Bruker TI Premier Nanoindenter. The radius of conical tip is 5.03 μm with a 60° apex angle, as shown later in Fig. 5(a). Nanoscratch tests were performed using a constant normal applied load (P), and the load was varied from 40 to 100 mN in 20mN increments. The scratch speed and scratch length were 8.33 μm/s and 250 μm, respectively. High magnification images were taken of the post-scratch sites using a Thermo Fischer FEI Quanta 3D scanning electron microscope. The scratch surface topography was then measured using a Bruker Dimension Icon atomic force microscope (AFM) with Scanasyst Air probes to quantify the residual scratch depth.

3. Results

3.1. Texture and microstructure development

XRD spectra for sputtered TiN coatings prepared using either conventional or pulsed DC magnetron sputtering in Fig. 1(a) show all films to be cubic TiN. Supplementary Fig. 2 shows the distinct golden color characteristic of TiN coatings. The conventional DC sputtered TiN has no texture, in contrast with a significant progression to strong (1 1 1) texture upon introducing a pulsed DC voltage profile. Interestingly, this sharp change in film texture is independent of substrate used, as presented in Supplementary Fig. 3, which shows the same evolution with pulse frequency on Si (1 1 1) and even amorphous SiO_2 substrates. This texture progression is further underscored in Fig. 1(b), which contains a plot of the peak intensity rations of TiN (1 1 1) and (2 0 0) against the pulse frequency. It is evident the use of pulsed DC leads to a consistent drastic change in film texture compared with the conventional DC sample (0 kHz).

Detailed TEM analysis was conducted to further assess the texture and microstructural evolution with increasing pulse frequency. Fig. 2 contains high angle annular dark field (HAADF) scanning transmission electron microscopy (STEM) images and inverse pole figure (IPF) maps comparing the conventional DC coating with those deposited using pulsed DC at 100–300 kHz pulse frequency. Corresponding bright field (BF) TEM images are provided in Supplementary Fig. 5. Fig. 2(a) shows that the microstructure of the conventional DC sample is composed of a

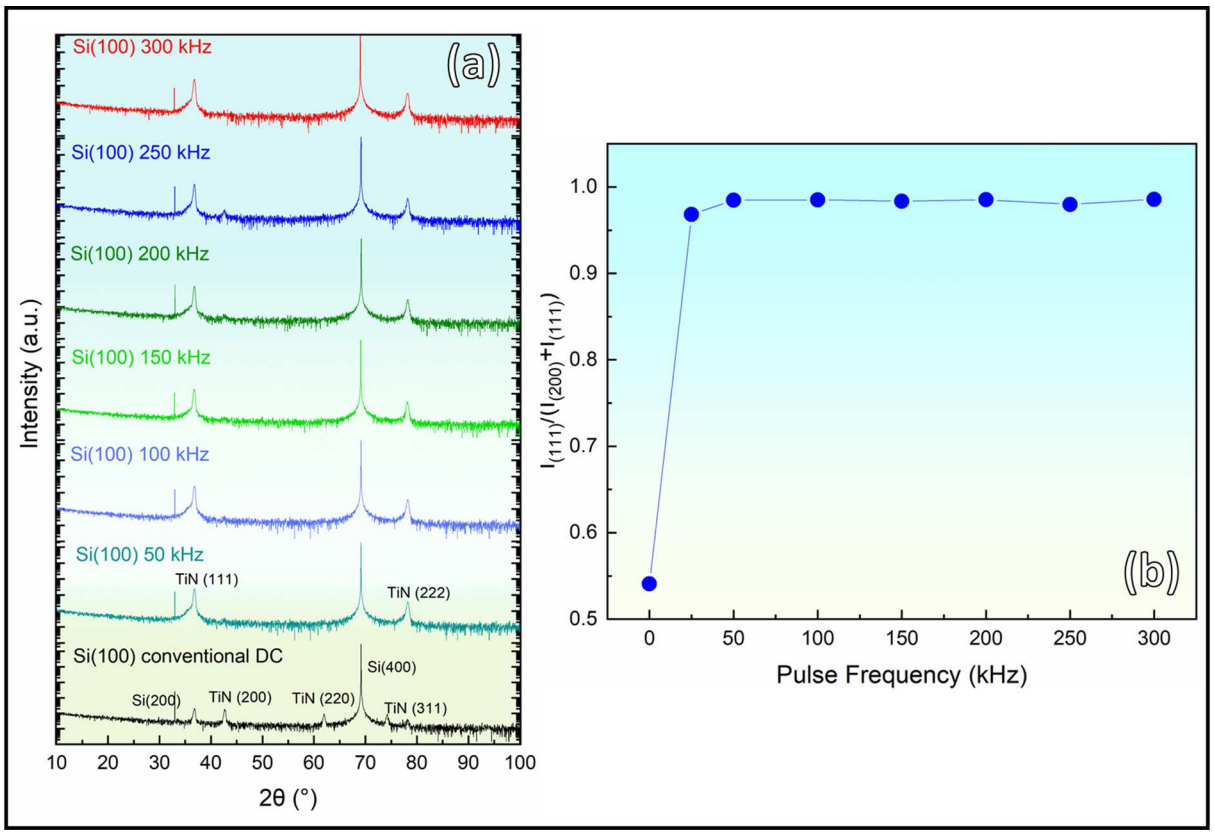

Fig. 1. (a) X-ray diffraction (XRD) patterns depicting the textural evolution of TiN coatings with increasing pulse frequency. (b) Evolution of the $I_{(1\,1\,1)}/(I_{(2\,0\,0)} + I_{(1\,1\,1)})$ x-ray peak intensity ratio with increasing pulse frequency.

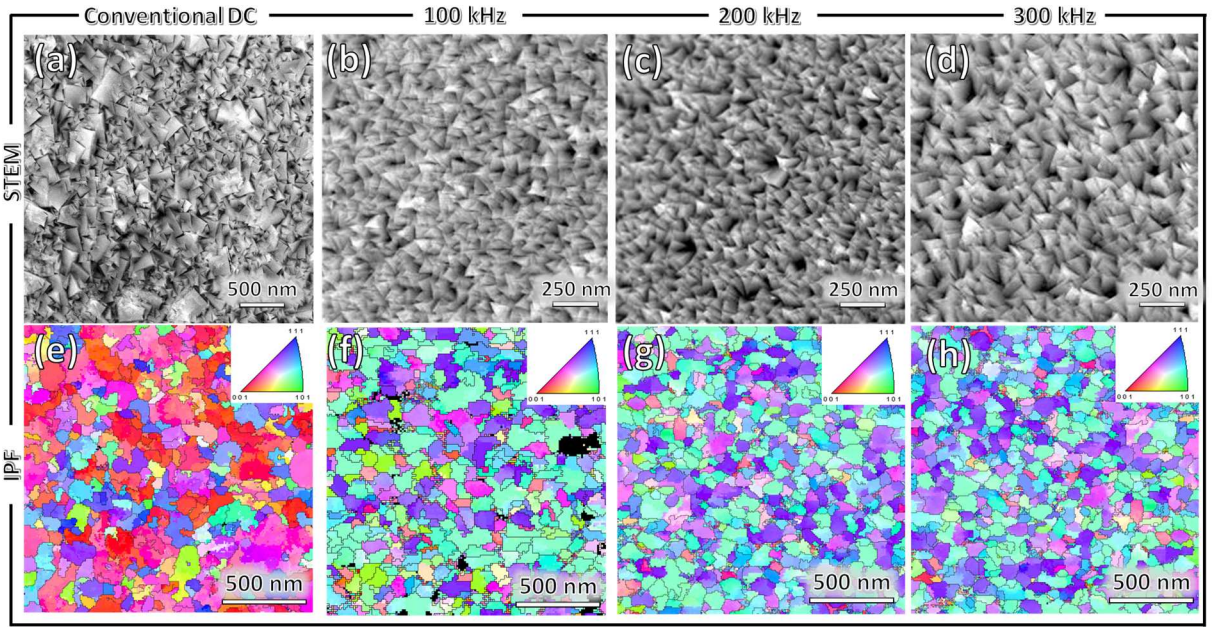

Fig. 2. (a-d) HAADF STEM plan-view images and (e-h) TEM ASTAR inverse pole figure (IPF) maps of TiN coatings deposited on Si (1 0 0) substrate using conventional DC and pulsed DC sputtering at various pulse frequencies.

mixture of large and small grains, with a majority of the small grains being triangular in shape suggesting a (1 1 1) orientation. Supplementary Fig. 4 reveals a bimodal grain size distribution in the Conventional DC sample. In comparison, Fig. 2(b-d) reveals the pulsed DC coatings are composed of almost completely fine triangular shaped grains. The grain size is reduced from ~240 nm in the conventional DC sample down to 80 nm in the 100 kHz pulse frequency sample, and to 50 nm in 300 kHz TiN. The IPF maps in Fig. 2(e-h) highlight the texture progression. Fig. 2 (e) shows a random mixture of grains with different orientations identified by the range of colors in the map for the conventional DC

specimen. The pulsed DC samples in Fig. 2(f-h) show a large fraction of (1 1 1) oriented grains, with very little variation in grain orientation. These IPF maps also confirm the progression of grain sizes presented previously. Supplementary Fig. 6 shows EDS maps collected using TEM proving the coatings in this study are all uniformly stochiometric TiN.

The same grain size and texture trends are identified in both the bright field (BF) and dark field (DF) XTEM images presented in Fig. 3. The microstructures of each coating are revealed to be columnar, with decreasing column size at higher pulse frequencies. The selected area diffraction (SAD) pattern in Fig. 3(a) shows randomly oriented columnar grains, while the pulsed DC SAD patterns show a stronger (1 1 1) texture outlined by the 6-sided pattern in Fig. 3(b) and (c). The DF-TEM images presented in Fig. 3(d-f) were all taken using a $\vec{g}$ of [2 0 0]. It is clear the pulsed DC films (Fig. 3(b, c)) have a finer columnar structure and there is a higher density of similarly textured columnar grains than in the conventional DC sample (Fig. 3(a)). A high-resolution TEM (HRTEM) micrograph in Fig. 4(a) details the cubic crystal structure of the conventional DC TiN coating. In comparison, Fig. 4(b) shows the TiN film deposited at 150 kHz is composed of regular FCC region and stacking faults. The inserted fast-Fourier transform (FFT) of the image show that these small stacking-fault regions possess an HCP crystal structure. These stacking fault regions are low in density and typically identified near columnar grain boundaries in the pulsed DC coatings.

3.2. Mechanical and tribological response

Nanoindentation was performed to link the mechanical response of these TiN coatings with the microstructural and texture evolution. A Hall-Petch plot is presented in Fig. 5 that compares the hardness evolution of the nitrides in this study with TiN coatings from literature fabricated using various deposition methods [65–67]. Notably, the TiN coatings from this study exhibit a greater hardness than prior TiN coatings at a similar grain size. Compared with the conventional sample with a hardness of 13 GPa, the hardness of TiN coatings increases monotonically with pulse frequency to ~20 GPa at 300 kHz; while the average grain size decreases with pulse frequency as shown in Supplementary Fig. 7.

Nanoscratch tests were conducted on each sample deposited in this study using a conical tip with a radius of 5.03 μm, and the test setup is illustrated in a schematic in Fig. 6(a). The total normal displacement (h) of the indenter tip increases monotonically with the normal applied load (P) as shown in Fig. 6(b). These normal displacements are also plotted against the lateral displacement in Supplementary Fig. 8 for each sample and normal applied load. These plots reveal a significant reduction in h for the TiN coatings deposited using pulsed DC compared with the conventional DC sample. The coefficients of friction (COF) are also compared as a function of P in Fig. 6(c). The overall trend indicates a higher pulse frequency slightly reduces the measured COF from 0.175 (Conventional DC) down to 0.145 (300 kHz). The governing wear mechanism will be discussed later. The COFs also slightly increase with applied load, but the increments are similar across the different samples.

The post-scratch sites were examined using both SEM and AFM imaging to assess the residual scratch sites qualitatively and quantitatively. Representative images were provided for selected pulsed DC specimens due to their similarity. Fig. 7(a) and (b) show SEM images comparing the post-scratch grooves of the conventional DC and 100 kHz pulse frequency samples tested at $P = 60$mN. The conventional DC post-scratch site in Fig. 7(a) contains extensive cracking and delamination of the TiN coating from the Si substrate, whereas the 100 kHz sample exhibits little breakdown of the film integrity at the same applied load. Both samples exhibit plasticity characterized by the pileup at the groove edges, which is also depicted in the AFM 3D surface profiles in Fig. 7(d) and (e). Fig. 7(c) depicts the measured residual scratch depths (h_R) as measured using AFM. The residual depth decreases with increasing pulse frequency and increases gradually with increasing normal applied load. Additionally, h_R increases significantly more with increasing P in the conventional sample than the pulse samples. The residual depth at an applied load of 100 mN for the conventional DC sample is 325 nm,

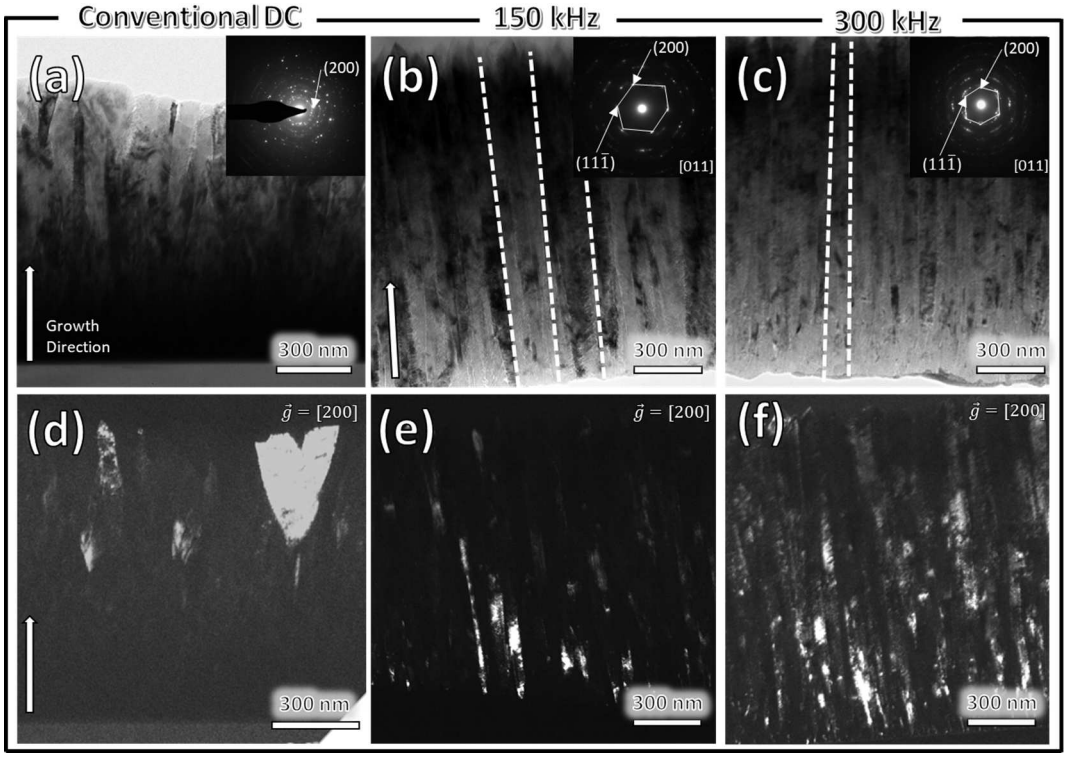

Fig. 3. (a-c) Bright-field XTEM images taken along the [0 1 1] zone axis with corresponding selected area diffraction (SAD) patterns for TiN coatings deposited using conventional DC and pulsed DC (150 and 300 kHz). (d-f) Dark-field XTEM images taken along $\vec{g}$ = [200] depicting the columnar grain refinement at higher pulse frequencies.

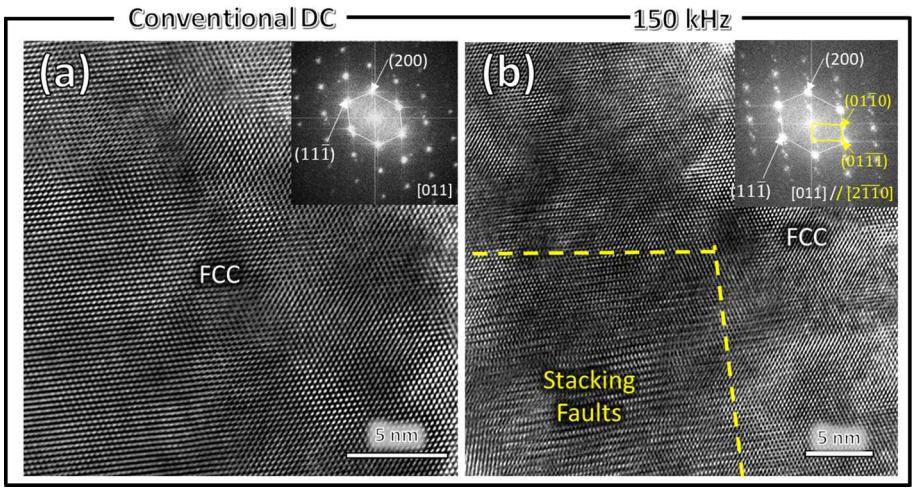

Fig. 4. (a) HRTEM image of pristine FCC lattice in TiN deposited using conventional DC. (b) HRTEM image of TiN deposited using pulsed DC with 150 kHz frequency revealing patches of stacking faults throughout the microstructure.

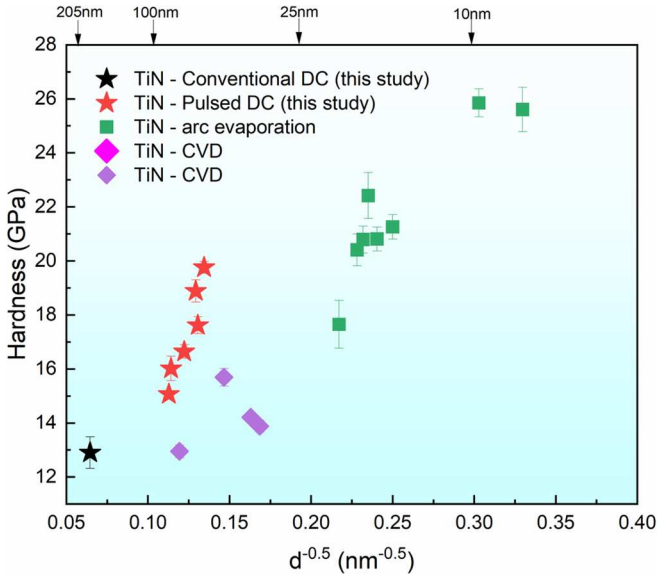

Fig. 5. Hall-Petch plot comparing the TiN films from this study with various TiN coatings fabricated using different methods in literature [60–62].

doubling that from the 300 kHz samples (~150 nm). Fig. 7(f), a comparison of the 2D AFM residual depth profiles, depicts the prominently greater residual depth and pileups in the conventional DC samples than the pulsed DC counterparts. Additional 3D AFM scans taken for the other samples (P = 60mN) are presented in Supplementary Fig. 10.

The residual scratch depth (h_R) measured using AFM can be used to calculate the contact radius and resulting wear area induced by nanoscratch testing. The residual contact radius (a_R) can be estimated as

$$a_R = \sqrt{2Rh_R - h_R^2} \tag{1}$$

where R is the reported radius of the conical diamond indenter tip (5.03 μm). Using a_R, the residual wear area (A_w) can be calculated as:

$$A_w = 2R^2 \sin^{-1}\left(\frac{a_R}{R}\right) - (R - h_R)a_R \tag{2}$$

The wear area is then used to determine the wear rate (W_R), which is defined as the volume of removed material per distance and normal applied load, and can be calculated using:

$$W_R = \frac{V}{xP} = \frac{A_w}{P} \tag{3}$$

where V is the wear volume, x is the lateral displacement during nanoscratch testing. It is clear the wear rates of the pulsed DC samples are significantly smaller than the conventional DC TiN sample for each value of P as shown in Fig. 8(b). The calculated values for the residual wear areas and wear rates are reported in Supplementary Table 1. Ultimately, the overall wear resistance (R_w) is able to be determined from the previously calculated tribological properties. The Archard equation can be used to calculate V induced during nanoscratch testing:

$$V = \frac{KP}{H}x \tag{4}$$

where K is the wear coefficient and H is the hardness. After combining Eq. 3 and 4, R_w can be determined using:

$$R_w = \frac{P}{A_W} = \frac{H}{K} \tag{5}$$

From Fig. 8(a), the plots of the normal applied load (P) against the wear area (A_w), the wear resistance (R_w) can be determined from the slope of these curves. Curve fitting was performed for each sample, and it is clear R_w for conventional DC TiN is significantly lower than each of the pulsed DC samples. The wear resistance is greater for specimens with higher hardness as shown in Fig. 8(c).

4. Discussion

4.1. Influence of pulsed DC deposition on film microstructures

4.1.1. Target surface conditions

Fabricating insulating compounds using reactive sputtering from conductive metal targets is often hindered by the process's hysteresis effect. As the reactive gas flow increases, the reactive gas pressure exhibits a hysteresis and ultimately avalanches from operating in "metallic" mode straight into the "reactive" (or "poisoned") mode [50,68]. This effect indicates the operation conditions are history dependent and provides a steep challenge to reaching optimal gas conditions for depositing high quality films. This phenomenon was thoroughly explored by Strijckmans et al. [47] and the interactions between the target material and the reactive gas are a driving factor in this hysteresis effect. Reactive sputtering of dielectric materials leads to the non-uniform accumulation of a non-conductive layer on the target surface and throughout the chamber, promoting mini- and macro-arcs

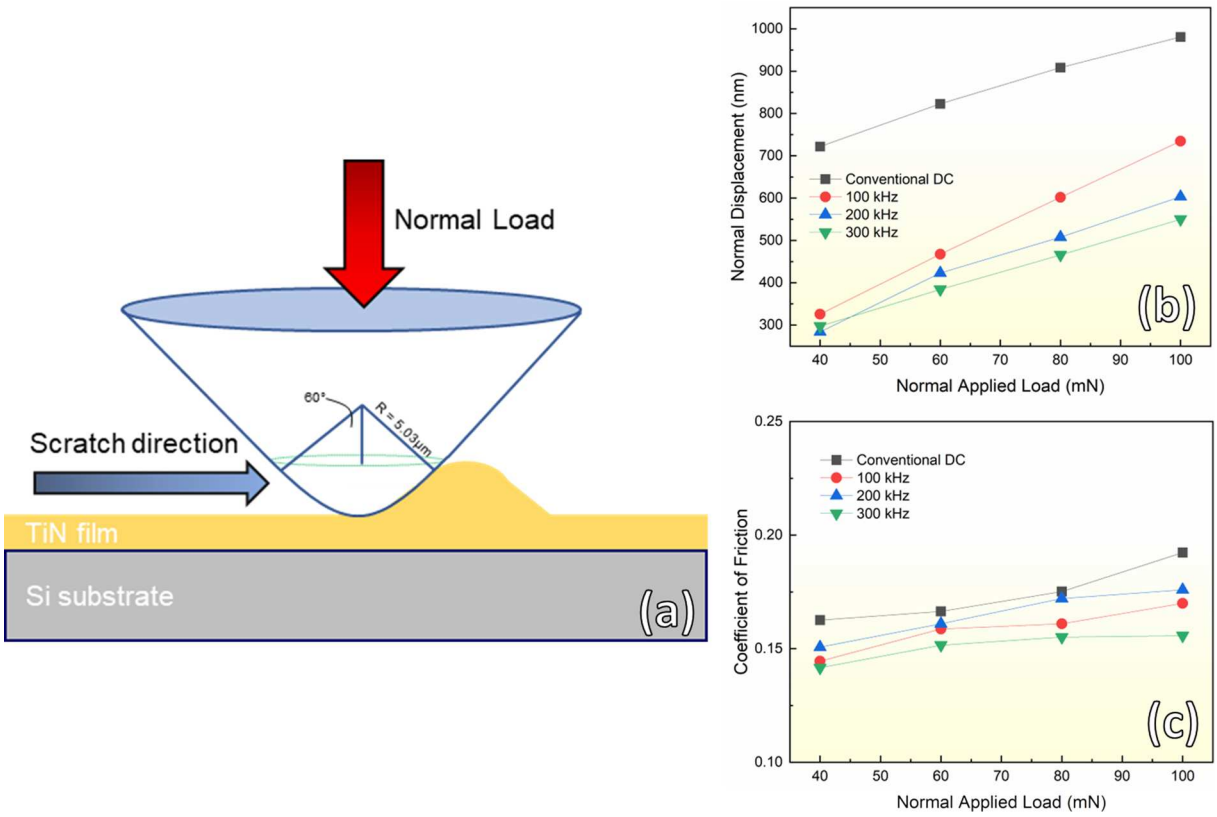

Fig. 6. (a) A schematic diagram illustrating the geometry of the high load scratch setup used to examine tribological properties of TiN coatings deposited with pulsed DC. (b) Variation in normal displacement measured during the nanoscratch tests with normal applied load. (c) Coefficient of friction (COF) measured during the nanoscratch tests at various normal applied loads.

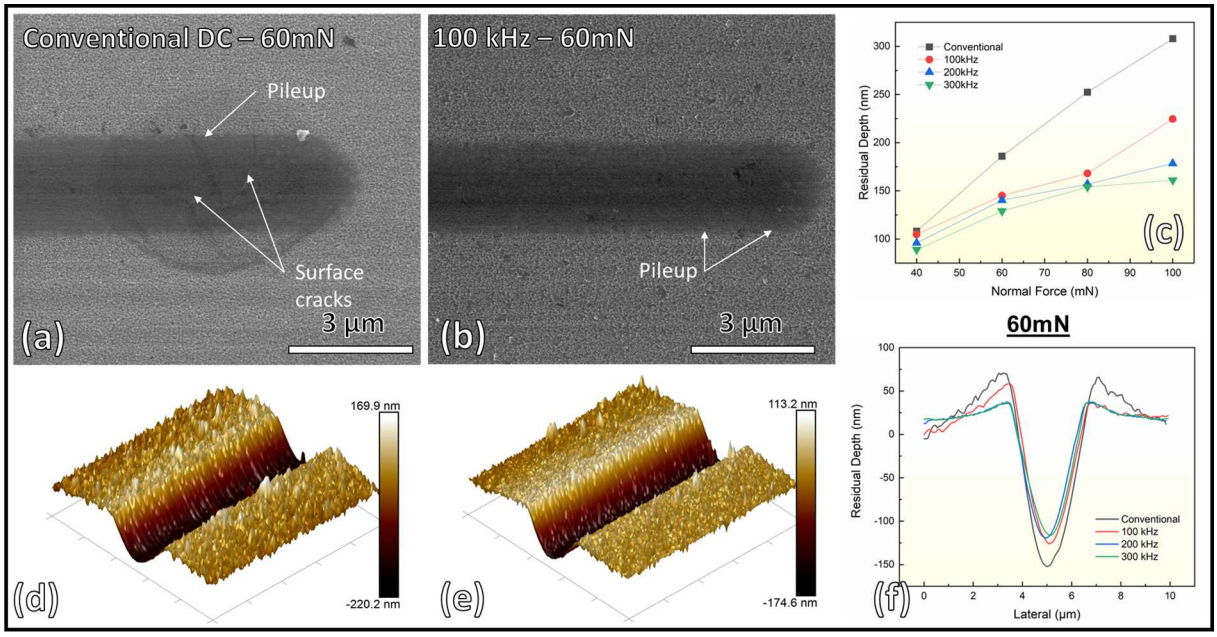

Fig. 7. (a-b) SEM images comparing the residual nanoscratch tracks of conventional DC with pulsed DC (100 kHz) tested at 60mN normal applied load. (c) Residual depths of the nanoscratch tracks on each TiN sample at various applied loads as measured using atomic force microscopy (AFM). (d-e) Topography maps for conventional (d) and 100 kHz pulse frequency (e) as measured using AFM. (f) Variation in the residual scratch depth profiles for each TiN sample tested at a normal applied load of 60 mN.

[13,52]. Arcing arises when the local electric field on the target surface overcomes the material's dielectric strength, promoting an avalanche of electron emission from the dielectric surface. Ultimately this arc event leads to the uneven removal of target material and particulates that are incorporated into the resulting film, degrading the overall film quality and texture [51]. Additionally, the hysteresis effect has a corresponding

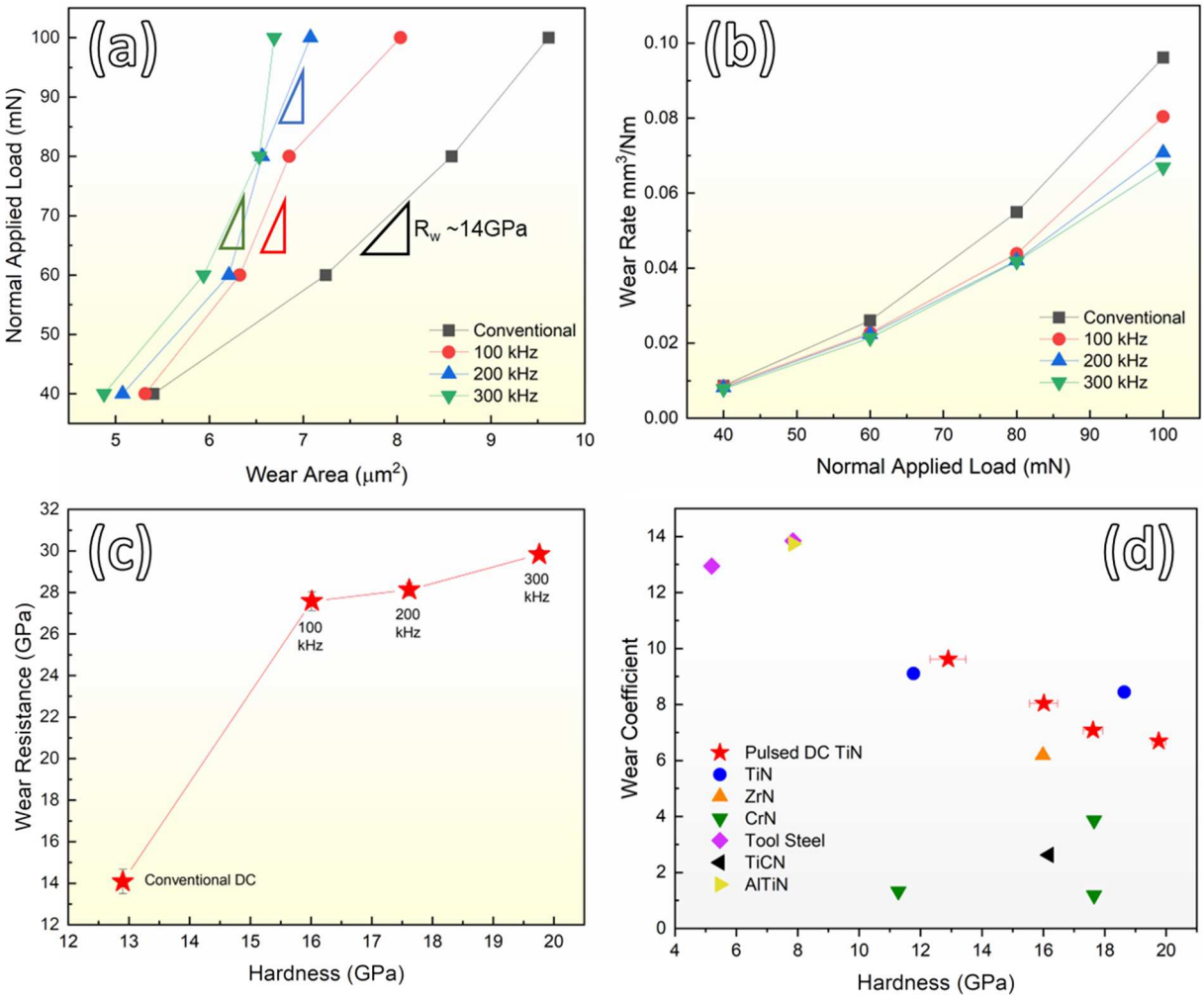

Fig. 8. (a) Progression of wear area calculated at various normal applied loads. (b) Change in wear rate with different pulse conditions at various applied loads. (c) Comparison of wear resistance of TiN coatings deposited at conventional and pulse DC conditions. (d) Literature comparison of the TiN presented in this study with literature for various nitride coatings and tool steels [79–84].

trend with decreasing erosion rate as the target surface is "poisoned" from a metallic source into a non-conductive compound. The Berg model of the reactive sputtering process provides multiple means of eliminating this hysteresis effect, including increasing pumping speeds drastically, significantly reducing target size, increasing substrate-to-target distance, or implementing a baffle to obstruct reactive gas flow to the target [47,52,68,69]. Most of these methods involve modifying the deposition chamber or components in a rather extreme way that hinders other aspects of the deposition process. In comparison, implementing a pulsed DC voltage profile to the target material is a far simpler means of restricting target poisoning and preventing process instabilities [19,70]. In pulsed DC mode, the polarity change in the voltage profile reduces target poisoning and other process instabilities that previously limited deposition [54]. The reverse bias attracts electrons back to the target surface and reduces charge buildup that promotes arc events. Schiller et al. demonstrated improved film quality and the removal of particulate formation in highly insulating Al_2O_3 and TiO_2 films deposited using pulsed DC reactive sputtering [71]. Belkind et al. [51] identified the critical pulse frequency to suppress arcing to be around 10 kHz for reactive sputtering of Al_2O_3. Fig. 9(a) illustrates the charge buildup seen in conventional DC reactive sputtering of TiN seen in this study. As TiN is far more conductive than Al_2O_3, it corresponds well that the resulting texture and microstructures are similar for the pulse frequencies presented here as the target conditions should be consistent, and little to no particulate formation is identified. There is an evident change in the microstructure between conventional DC and the pulsed DC as presented in the HAADF images in Fig. 2. Fig. 2(a) reveals a mixture of large and small grains in conventional DC TiN, as well as randomized texture as presented using IPF maps in Fig. 2(e), whereas the pulsed DC TiN coatings all have strong (1 1 1) texture and much smaller grain sizes (Fig. 2f-h, and Supp. Fig. 7). Additionally, there does appear to be a higher level of porosity in the conventional DC films than any of the pulsed DC films. Hence, it is evident that the pulsed DC during reactive sputtering has promoted clear microstructural changes from the conventional DC sputtering.

4.1.2. *Plasma conditions*

Sputtered film microstructure, and ultimately properties, are largely altered through controlling the energy delivered to the growing film through ion bombardment [70]. The energy and flux of the bombarding ions are both highly dependent on the plasma conditions around the substrate, so tailoring the plasma conditions directly influence the resulting film structure and properties. Kelly and Arnell [72] documented a structure zone model that indicates the substrate homologous temperature, the flux ratio of ions and the ion bombardment energy of ions onto the substrate strongly influence the resulting film microstructure. As the substrate temperature is relatively low (~0.15 T_m of TiN) and held constant across all experiments presented here, the energies and ratios of the ions within the plasma are the driving factors behind the microstructural development in TiN deposited using pulsed

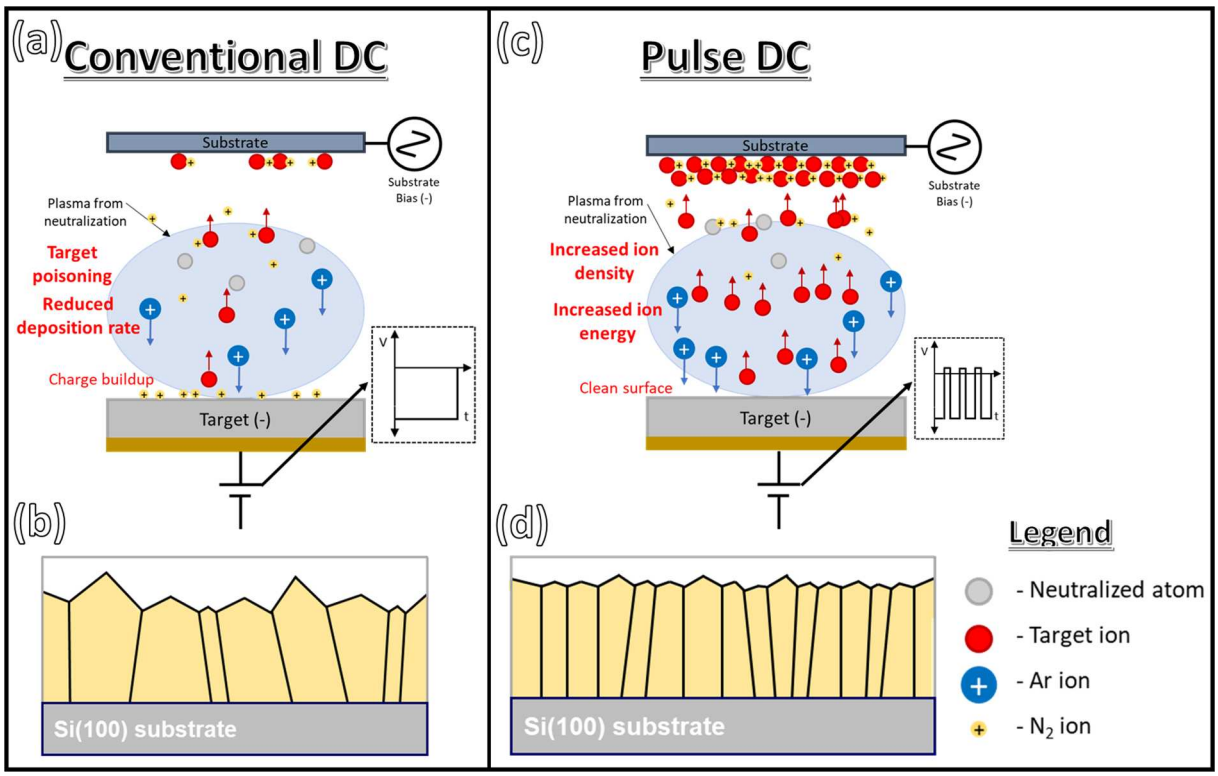

Fig. 9. (a-b) Schematics depicting the change in plasma conditions experienced during magnetron sputtering using conventional DC and the resulting film microstructure. (c-d) Schematics showing the change in plasma conditions experienced during pulsed DC magnetron sputtering and the resulting film microstructure.

DC. TEM analyses in Figs. 2 and 3 depict a clear trend of columnar grain refinement and texture enhancement with increasing pulse frequency. Literature establishes a similar trend as pulse frequency directly impacts nitride microstructure and texture, and the structure progression is intimately tied to the aforementioned plasma conditions [56].

Previous explorations of plasma conditions during reactive sputtering have indicated how a pulsed target voltage profile directly affects the ions populating the plasma. Kinetically, the pulse-off time (order of μs) is not long enough to completely interrupt plasma and film growth [73]. The influence of using a pulsed DC power supply manifests itself in altering the bombarding ion energy and flux ratios [56,70]. Based on Langmuir probe measurements, Bradley et al [74] observed changes in the plasma potential and the electron density and temperature during sputtering of an aluminum target using pulsed DC. They reported a notable increase in the electron temperature immediately following the voltage reversal into the "pulse-on" condition, along with a boost in density of high and medium energy ions [74]. Additionally, the Langmuir probe measurements revealed a higher density of low energy ions generated during the "voltage-on" period than surrounding the pulse switch [74]. Increasing the electron temperature promotes a more chemically active plasma that enhances the reaction between Ti^+ and N^+ ions and could improve film stoichiometry. The increase in high-energy ions leads to a higher bombardment energy and ion flux for the substrate and film [70,74]. This trend is similar to what has been reported previously related to applying a substrate bias [75] or reducing the substrate-to-target distance [28]. By reducing the substrate-to-target distance, Barnes et al. were able to deliver higher energy ions to the TiO_2 film and induce crystallization into previously amorphous coatings [28]. Ultimately, depositing films at higher pulse frequencies provides more instances of bombardment of higher energy ions. Similar differences are expected in films deposited at higher deposition rates, however in this work the deposition rate was monitored *in-situ* using a quartz crystal rate monitor and was consistent across all deposited coatings and was not a major factor on the resulting film microstructures.

The columnar grain refinement and texture enhancement identified in the TEM analyses of Figs. 2 and 3 as well as the IPF maps in Fig. 2 can be attributed to the changing plasma conditions induced by altering the pulse frequency. The relationship between microstructure and plasma conditions is depicted in Fig. 9(a-d). Since each other process variable is held constant, the use of a pulsed DC power supply is strongly suggested to be the main factor behind this texture change. When directly comparing the TiN film microstructure across different pulse frequencies, they are morphologically similar and exhibit a relatively linear decrease in grain size with increasing pulse frequency. As the pulse frequency is increased, the plasma experiences a larger frequency of events where high energy ions are generated and bombard the growing film [74]. This phenomenon is similar to applying a negative substrate bias, which attracts and accelerates a larger density of bombarding ions onto the substrate. Petrov et al. [75] applied varying levels of negative substrate bias during deposition of TiN and reported a decrease in grain size at larger biases. The grain size reduction was attributed to re-nucleation occurring due to the increase in point defects originating from the ion bombardment [75]. These defects alter the diffusion of deposited atoms and enable both grain size reduction and the development of the preferred (1 1 1) texture. Kajikawa et al. identified surface diffusion as a key parameter driving the development of texture in nitride coatings [31]. Monte Carlo simulations have demonstrated an enhancement of adatom diffusivity when the kinetic energy of the bombarding ion is increased [76]. These findings support the trends reported in pulse DC sputtered TiN as increasing pulse frequency promotes high energy ion formation that in turn bombards the substrate and enhance adatom diffusivity. The pulse frequencies probed in this work (up to 300 kHz) are beyond the typical operation regime of pulse DC power supplies (70–100 kHz). Ultimately, this pulsed DC process drives the reduction in grain size and promotes (1 1 1) texture as presented in Fig. 2. By increasing the instances of high energy ion generation, the microstructure and hardness are further tuned resulting in films with improved wear resistance, as shown in Fig. 8. Expanding the pulse

frequency range enables further tunability of TiN film structure and mechanical properties. In addition to these microstructural trends, small regions composed of a high density of stacking faults (Fig. 4(b)) were identified in the pulse DC samples. It is possible that while the adatom diffusivity is enhanced, the extremely high quench rates characteristic of magnetron sputtering trap these stacking faults during deposition. It is also possible that the strong (1 1 1) texture leads to a higher density of stacking faults which form on the closely packed planes. A more thorough future study on the relationship between these stacking fault arrays and pulse DC parameters is necessary.

4.2. Improved wear properties of pulsed DC TiN coating

Nitrides have been widely investigated due to their impressive wear resistance and mechanical stability. Coefficient of friction (COF) is a common property used to assess the resistance of a material to wear deformation as it describes the resistance to relative motion between two contacting surfaces [21,77]. Amontons and Coulomb's friction law identifies the relationship between the normal applied force (F_N) and the tangentially applied force (F_t) as $F_N = \mu \cdot F_t$, where μ is the COF [78]. In nanoscratch testing, the friction force governing the COF of TiN can be derived from two main processes, the adhesion between the indenter tip and the film surface, and the deformation of the TiN coating [77,79]. As these are two independent processes, the COF can be assumed to be the sum of the adhesion and deformation components ($\mu = \mu_{adh} + \mu_{def}$) [21]. The adhesion component (μ_{adh}) is controlled by a materials interfacial shear strength and its influence on COF has been shown through simulations to be negligible [17,21] when the applied load causes plastic deformation, which is clearly identified here by the pileup shown in the SEM images and AFM scans in Fig. 7. Therefore, the evolution of the COF seen in Fig. 6(c) originates from the deformation component (μ_{def}) of the friction force, which is strongly related to the materials mechanical properties [80].

The COF decreases from 0.175 for conventional DC TiN to 0.14 when deposited using 300 kHz pulsed DC. Tribological properties are often dependent on the hardness of the tested material and increasing a film's hardness typically improves both COF and wear resistance. In the previous section, the plasma conditions during pulsed DC sputtering of TiN were related to the evolving texture and reduced grain size. A materials hardness are intimately linked to the grain size (d) through the Hall-Petch relationship [81–83]. The Hall-Petch plot in Fig. 5 highlights the hardness enhancement seen at smaller grain sizes (higher pulse frequencies) when compared with other TiN coatings fabricated using various deposition methods. The reactively sputtered films presented in this work reach a higher hardness than coatings deposited using CVD that possess similar grain sizes. This is captured in an increased Hall-Petch coefficient in this study ($k_y \sim 66.2$ GPa·nm$^{-1/2}$) compared with literature ($k_y \sim 54.4$ GPa·nm$^{-1/2}$), indicating an increase in barrier strength to dislocation motion. The improved Hall-Petch coefficient is likely linked with the enhanced texture. The increment in Hall-Petch coefficient could be induced by the strong (1 1 1) texture promoting stronger boundary types or from the small patches of stacking faults presented in Fig. 4(b) in the pulsed DC samples. One other observation that could factor into the rise in hardness is the reduction in film porosity due to the shadowing effect during film growth [76]. In the PVTEM image in Fig. 2(a), there is a larger fraction of pores between the mixture of large and small grains in the conventional DC TiN. In comparison, the pulsed DC TiN samples have a reduction in porosity linked with the increase in adatom diffusivity due to the high bombarding ion energy [76]. Overall, a higher hardness indicates a reduction in plastic deformation experienced by the pulse DC TiN coating during nanoscratch testing which reduces the COF. Additionally, Fig. 8(d) compares the wear coefficient and hardness of the nitride coatings from this study with various wear resistant materials from literature [84–89]. This parameter directly relates to the rate of material loss due to wear, so a lower wear coefficient is desirable. As can be seen in Fig. 8(d), the pulse DC TiN coatings in this study outperform the other TiN coatings (wear coefficient reduced to ~7), while being comparable with ZrN and various complex nitrides. The boost in wear resistance is obvious and clearly highlights the improvement of tribological and mechanical properties that can be provided by using pulsed DC magnetron sputtering of TiN coatings. By applying high pulse frequencies (i.e., 300 kHz), the wear resistance of the coating can further improve.

To further understand the improved wear resistance of the pulsed DC sputtered TiN, it is necessary to discuss the various mechanisms governing wear during nanoscratch testing. Nanoscratch testing induces various deformation mechanisms, including ploughing, cutting, shearing, and cracking. As no cutting chips [80] were identified in the post-scratch SEM images in Fig. 7(a-b), cutting is not considered to be a major operating mechanism during nanoscratch of TiN. Additionally, Zhang et al. [17] identified shear bands in NT Al-Ni alloys after nanoscratch testing, however none were seen here. Ploughing is assumed to be the dominant mechanisms in ductile materials [80,90]. Based on the pileup identified in Fig. 7, ploughing is like to be the major mechanism operating in TiN. Both COF and wear resistance are dependent on the ploughing mechanism. Specifically, the ploughing COF (μ_{pl}) has been related to nanoscratch parameters including tip geometry, penetration depth and elastic recovery rate [21,91], and a model was proposed to determine μ_{pl} for a conical indenter tip geometry:

$$\mu_{pl} = \frac{2}{\pi a_i^2}\left(R^2 \sin^{-1}\left(\frac{a_i}{R}\right)\right) - a_i\sqrt{R^2 - a_i^2} \quad (5)$$

where a_i is the radius of scratch profile, and R is the conical tip radius. This model suggests that μ_{pl} will increase with increasing penetration depth until it approaches R where it plateaus. As the indentation depth in this study is on the order of 100 s of nm, it supports the COF values determined here (0.14–0.18) as well as the positive slope of the COF vs normal displacement curve in Fig. 6(c). Additionally, the extent of ploughing governs the wear resistance (R_w) and can help explain the boost in R_w seen in pulsed DC sputtered TiN in Fig. 8(c). 2D profiles of AFM scans for each sample tested with a normal applied load of 60mN show a decrease in material pileup with increasing pulse frequency. The residual depth of the scratch trench was also shown to be reduced in coatings deposited with a higher pulse frequency in Fig. 7(c). This observation is an indication of a reduction in plastic deformation in pulsed DC TiN as well as smaller wear volumes at higher pulse frequencies, and it corresponds well with the increasing hardness at high pulse frequencies. This variation manifests itself in a higher R_w as shown in Fig. 8(c) and can be directly linked back to the changing plasma conditions induced by pulse frequency. Fig. 8(d) also provides insight into the improved wear properties as the wear coefficient, which is related to the material loss experienced during wear. As Fig. 8(d) depicts, pulse DC TiN outperforms conventional DC TiN and TiN reported in literature. Overall, this work indicates wear resistant coatings deposited using reactive magnetron sputtering can be improved by using a pulsed DC power supply.

5. Conclusion

Reactive magnetron sputtering was used to fabricate TiN coatings using both conventional and pulsed DC voltage profiles during sputtering. XRD and extensive microscopy analyses detailed the strong (1 1 1) texture promoted in TiN films deposited using pulsed DC. Increasing the pulse frequency led to significant grain refinement that worked simultaneously with the stronger texture to bolster the mechanical and tribological properties of TiN. These changes were attributed to the impact a pulsed DC voltage profile has on the plasma conditions, specifically the bombarding ion density and energy. This study provides a strong account of the ability to tailor film structure and properties of reactively sputtered compounds using a pulsed DC power supply.

CRediT authorship contribution statement

N.A. Richter: Conceptualization, Methodology, Validation, Formal analysis, Investigation, Writing – original draft, Writing – review & editing, Visualization. **B. Yang:** Formal analysis, Investigation. **J.P. Barnard:** Formal analysis, Investigation. **T. Niu:** Formal analysis, Investigation. **X. Sheng:** Formal analysis, Investigation. **D. Shaw:** Conceptualization, Writing – review & editing, Project administration, Funding acquisition, Supervision. **M. Watanabe:** Conceptualization, Writing – review & editing, Project administration, Funding acquisition, Supervision. **G. Rane:** Methodology, Validation, Supervision. **U. Krause:** Methodology, Validation, Supervision. **P. Dürrenfeld:** Methodology, Validation, Supervision. **H. Wang:** Project administration, Funding acquisition. **X. Zhang:** Conceptualization, Writing – review & editing, Project administration, Funding acquisition, Supervision.

Declaration of Competing Interest

The authors declare that they have no known competing financial interests or personal relationships that could have appeared to influence the work reported in this paper.

Data availability

Data will be made available on request.

Acknowledgements

This work is supported by Advanced Energy Industries, Inc. The ASTAR crystal orientation system in TEM microscope is supported by ONR-DURIP award N00014-17-1-2921. J. B. and H.W. acknowledge the support from the U.S. National Science Foundation (DMR-2016453) for the related nitride film property measurements. We would also like to acknowledge the microscopy center of the School of Materials Engineering at Purdue University.

Appendix A. Supplementary material

Supplementary data to this article can be found online at https://doi.org/10.1016/j.apsusc.2023.157709.

References

[1] K. Holmberg, P. Andersson, N.-O. Nylund, K. Mäkelä, A. Erdemir, Global energy consumption due to friction in trucks and buses, Tribol. Int. 78 (2014) 94–114, https://doi.org/10.1016/j.triboint.2014.05.004.
[2] H.P. Jost, J. Schofield, Energy saving through tribology: a techno-economic study, Proc. Inst. Mech. Eng. 195 (1981) 151–173, doi: 10.1243/PIME_PROC_1981_195_016_02.
[3] A. Barata, L. Cunha, C. Moura, Characterisation of chromium nitride films produced by PVD techniques, Thin Solid Films 398–399 (2001) 501–506, https://doi.org/10.1016/S0040-6090(01)01498-5.
[4] P. Patsalas, C. Charitidis, S. Logothetidis, The effect of substrate temperature and biasing on the mechanical properties and structure of sputtered titanium nitride thin films, Surf. Coat. Technol. 125 (2000) 335–340, https://doi.org/10.1016/S0257-8972(99)00606-4.
[5] S. PalDey, S.C. Deevi, Single layer and multilayer wear resistant coatings of (Ti, Al)N: a review, Mater. Sci. Eng. A 342 (2003) 58–79, https://doi.org/10.1016/S0921-5093(02)00259-9.
[6] S. Das, S. Guha, R. Ghadai, A. Sharma, Influence of nitrogen gas over microstructural, vibrational and mechanical properties of CVD Titanium nitride (TiN) thin film coating, Ceram. Int. 47 (2021) 16809–16819, https://doi.org/10.1016/j.ceramint.2021.02.254.
[7] T. Ishigaki, S. Tatsuoka, K. Sato, K. Yanagisawa, K. Yamaguchi, S. Nishida, Influence of the Al content on mechanical properties of CVD aluminum titanium nitride coatings, Int. J. Refract Metal Hard Mater. 71 (2018) 227–231, https://doi.org/10.1016/j.ijrmhm.2017.11.028.
[8] P. LeClair, G.P. Berera, J.S. Moodera, Titanium nitride thin films obtained by a modified physical vapor deposition process, Thin Solid Films 376 (2000) 9–15, https://doi.org/10.1016/S0040-6090(00)01192-5.
[9] H.-E. Cheng, Y.-W. Wen, Correlation between process parameters, microstructure and hardness of titanium nitride films by chemical vapor deposition, Surf. Coat. Technol. 179 (2004) 103–109, https://doi.org/10.1016/S0257-8972(03)00789-8.
[10] O.R. Shojaei, A. Karimi, Comparison of mechanical properties of TiN thin films using nanoindentation and bulge test, Thin Solid Films 332 (1998) 202–208, https://doi.org/10.1016/S0040-6090(98)01057-8.
[11] J.M. Lackner, Industrially-scaled large-area and high-rate tribological coating by Pulsed Laser Deposition, Surf. Coat. Technol. 200 (2005) 1439–1444, https://doi.org/10.1016/j.surfcoat.2005.08.029.
[12] S. Zhang, F. Yan, Y. Yang, M. Yan, Y. Zhang, J. Guo, H. Li, Effects of sputtering gas on microstructure and tribological properties of titanium nitride films, Appl. Surf. Sci. 488 (2019) 61–69, https://doi.org/10.1016/j.apsusc.2019.05.148.
[13] P.J. Kelly, C.F. Beevers, P.S. Henderson, R.D. Arnell, J.W. Bradley, H. Bäcker, A comparison of the properties of titanium-based films produced by pulsed and continuous DC magnetron sputtering, Surf. Coat. Technol. 174–175 (2003) 795–800, https://doi.org/10.1016/S0257-8972(03)00356-6.
[14] N.W. Cheung, H. von Seefeld, M. Nicolet, F. Ho, P. Iles, Thermal stability of titanium nitride for shallow junction solar cell contacts, J. Appl. Phys. 52 (1981) 4297–4299, https://doi.org/10.1063/1.329283.
[15] P. Roquiny, F. Bodart, G. Terwagne, Colour control of titanium nitride coatings produced by reactive magnetron sputtering at temperature less than 100°C, Surf. Coat. Technol. 116–119 (1999) 278–283, https://doi.org/10.1016/S0257-8972(99)00076-6.
[16] K. Holmberg, A. Erdemir, The impact of tribology on energy use and CO2 emission globally and in combustion engine and electric cars, Tribol. Int. 135 (2019) 389–396, https://doi.org/10.1016/j.triboint.2019.03.024.
[17] Y. Zhang, T. Niu, N.A. Richter, T. Sun, N. Li, H. Wang, X. Zhang, Tribological behaviors of nanotwinned Al alloys, Appl. Surf. Sci. (2022) 154108, doi: 10.1016/j.apsusc.2022.154108.
[18] S. Datta, M. Das, V.K. Balla, S. Bodhak, V.K. Murugesan, Mechanical, wear, corrosion and biological properties of arc deposited titanium nitride coatings, Surf. Coat. Technol. 344 (2018) 214–222, https://doi.org/10.1016/j.surfcoat.2018.03.019.
[19] P.J. Kelly, T. vom Braucke, Z. Liu, R.D. Arnell, E.D. Doyle, Pulsed DC titanium nitride coatings for improved tribological performance and tool life, Surf. Coat. Technol. 202 (2007) 774–780, https://doi.org/10.1016/j.surfcoat.2007.07.047.
[20] B.D. Beake, A.J. Harris, T.W. Liskiewicz, Review of recent progress in nanoscratch testing, Tribol. Mater. Surf. Interfaces 7 (2013) 87–96, https://doi.org/10.1179/1751584X13Y.0000000037.
[21] S. Lafaye, M. Troyon, On the friction behaviour in nanoscratch testing, Wear 261 (2006) 905–913, https://doi.org/10.1016/j.wear.2006.01.036.
[22] H.R. Chamani, M.R. Ayatollahi, The effect of Berkovich tip orientations on friction coefficient in nanoscratch testing of metals, Tribol. Int. 103 (2016) 25–36, https://doi.org/10.1016/j.triboint.2016.06.036.
[23] B.D. Beake, A.A. Ogwu, T. Wagner, Influence of experimental factors and film thickness on the measured critical load in the nanoscratch test, Mater. Sci. Eng. A 423 (2006) 70–73, https://doi.org/10.1016/j.msea.2005.09.121.
[24] A.M. Hodge, T.G. Nieh, Evaluating abrasive wear of amorphous alloys using nanoscratch technique, Intermetallics 12 (2004) 741–748, https://doi.org/10.1016/j.intermet.2004.02.014.
[25] S.M. Noh, J.W. Lee, J.H. Nam, J.M. Park, H.W. Jung, Analysis of scratch characteristics of automotive clearcoats containing silane modified blocked isocyanates via carwash and nano-scratch tests, Prog. Org. Coat. 74 (2012) 192–203, https://doi.org/10.1016/j.porgcoat.2011.12.009.
[26] Z. Peng, H. Miao, L. Qi, S. Yang, C. Liu, Hard and wear-resistant titanium nitride coatings for cemented carbide cutting tools by pulsed high energy density plasma, Acta Mater. 51 (2003) 3085–3094, https://doi.org/10.1016/S1359-6454(03)00119-8.
[27] A.A.C. Recco, C.C. Viáfara, A. Sinatora, A.P. Tschiptschin, Energy dissipation in depth-sensing indentation as a characteristic of the nanoscratch behavior of coatings, Wear 267 (2009) 1146–1152, https://doi.org/10.1016/j.wear.2009.01.043.
[28] M.C. Barnes, A.R. Gerson, S. Kumar, N.-M. Hwang, The mechanism of TiO2 deposition by direct current magnetron reactive sputtering, Thin Solid Films 446 (2004) 29–36, https://doi.org/10.1016/S0040-6090(03)01279-3.
[29] R. Banerjee, R. Chandra, P. Ayyub, Influence of the sputtering gas on the preferred orientation of nanocrystalline titanium nitride thin films, Thin Solid Films 405 (2002) 64–72, https://doi.org/10.1016/S0040-6090(01)01705-9.
[30] I. Petrov, P.B. Barna, L. Hultman, J.E. Greene, Microstructural evolution during film growth, J. Vac. Sci. Technol. A 21 (2003) S117–S128, https://doi.org/10.1116/1.1601610.
[31] Y. Kajikawa, S. Noda, H. Komiyama, Comprehensive perspective on the mechanism of preferred orientation in reactive-sputter-deposited nitrides, J. Vac. Sci. Technol. A 21 (2003) 1943, https://doi.org/10.1116/1.1619414.
[32] S. Mahieu, D. Depla, Reactive sputter deposition of TiN layers: Modelling the growth by characterization of particle fluxes towards the substrate, J. Phys. D Appl. Phys. 42 (2009), https://doi.org/10.1088/0022-3727/42/5/053002.
[33] T.Q. Li, S. Noda, Y. Tsuji, T. Ohsawa, H. Komiyama, Initial growth and texture formation during reactive magnetron sputtering of TiN on Si(111), J. Vac. Sci. Technol. A 20 (2002) 583–588, https://doi.org/10.1116/1.1458944.
[34] H. Onoda, M. Kageyama, K. Hashimoto, Al-Si crystallographic-orientation transition in Al-Si/TiN layered structures and electromigration performance as interconnects, J. Appl. Phys. 77 (1995) 885–892, https://doi.org/10.1063/1.359014.
[35] J.-E. Sundgren, Structure and properties of TiN coatings, Thin Solid Films 128 (1985) 21–44, https://doi.org/10.1016/0040-6090(85)90333-5.
[36] G. Beensh-Marchwicka, L. Kròl-Stępniewska, W. Posadowski, Structure of thin films prepared by the cosputtering of titanium and aluminium or titanium and

silicon, Thin Solid Films 82 (1981) 313–320, https://doi.org/10.1016/0040-6090(81)90474-0.
[37] M.-K. Lee, H.-S. Kang, W.-W. Kim, J.-S. Kim, W.-J. Lee, Characteristics of TiN film deposited on stellite using reactive magnetron sputter ion plating, J. Mater. Res. 12 (1997) 2393–2400, https://doi.org/10.1557/JMR.1997.0317.
[38] X.-H. Xu, H.-S. Wu, C.-J. Zhang, Z.-H. Jin, Morphological properties of AlN piezoelectric thin films deposited by DC reactive magnetron sputtering, Thin Solid Films 388 (2001) 62–67, https://doi.org/10.1016/S0040-6090(00)01914-3.
[39] Y.M. Chen, G.P. Yu, J.H. Huang, Characterizing the effects of multiprocess parameters on the preferred orientation of TiN coating using a combined index, Vacuum 66 (2002) 19–25, https://doi.org/10.1016/S0042-207X(01)00416-X.
[40] N. Ghobadi, M. Ganji, C. Luna, A. Arman, A. Ahmadpourian, Effects of substrate temperature on the properties of sputtered TiN thin films, J Mater Sci: Mater Electron. 27 (2016) 2800–2808, https://doi.org/10.1007/s10854-015-4093-x.
[41] M.K. Hibbs, B.O. Johansson, J.-E. Sundgren, U. Helmersson, Effects of substrate temperature and substrate material on the structure of reactively sputtered TiN films, Thin Solid Films 122 (1984) 115–129, https://doi.org/10.1016/0040-6090(84)90003-8.
[42] H.-C. Lee, J.-Y. Lee, Effects of sputtering pressure and nitrogen concentration on the preferred orientation of AlN thin films, J Mater Sci: Mater Electron. 5 (1994), https://doi.org/10.1007/BF00186189.
[43] M. Ishihara, S.J. Li, H. Yumoto, K. Akashi, Y. Ide, Control of preferential orientation of AlN films prepared by the reactive sputtering method, Thin Solid Films 316 (1998) 152–157, https://doi.org/10.1016/S0040-6090(98)00406-4.
[44] Y. Xi, K. Gao, X. Pang, H. Yang, X. Xiong, H. Li, A.A. Volinsky, Film thickness effect on texture and residual stress sign transition in sputtered TiN thin films, Ceram. Int. 43 (2017) 11992–11997, https://doi.org/10.1016/j.ceramint.2017.06.050.
[45] J.E. Greene, J.-E. Sundgren, L. Hultman, I. Petrov, D.B. Bergstrom, Development of preferred orientation in polycrystalline TiN layers grown by ultrahigh vacuum reactive magnetron sputtering, Appl. Phys. Lett. 67 (1995) 2928–2930, https://doi.org/10.1063/1.114845.
[46] H. Liang, J. Xu, D. Zhou, X. Sun, S. Chu, Y. Bai, Thickness dependent microstructural and electrical properties of TiN thin films prepared by DC reactive magnetron sputtering, Ceram. Int. 42 (2016) 2642–2647, https://doi.org/10.1016/j.ceramint.2015.10.070.
[47] K. Strijckmans, R. Schelfhout, D. Depla, Tutorial: Hysteresis during the reactive magnetron sputtering process, J. Appl. Phys. 124 (2018), https://doi.org/10.1063/1.5042084.
[48] J. Musil, P. Baroch, J. Vlček, K.H. Nam, J.G. Han, Reactive magnetron sputtering of thin films: present status and trends, Thin Solid Films 475 (2005) 208–218, https://doi.org/10.1016/j.tsf.2004.07.041.
[49] W.D. Sproul, D.J. Christie, D.C. Carter, Control of reactive sputtering processes, Thin Solid Films 491 (2005) 1–17, https://doi.org/10.1016/j.tsf.2005.05.022.
[50] S. Berg, T. Nyberg, Fundamental understanding and modeling of reactive sputtering processes, Thin Solid Films 476 (2005) 215–230, https://doi.org/10.1016/j.tsf.2004.10.051.
[51] A. Belkind, A. Freilich, J. Lopez, Z. Zhao, W. Zhu, K. Becker, Characterization of pulsed dc magnetron sputtering plasmas, New J. Phys. 7 (2005) 90, https://doi.org/10.1088/1367-2630/7/1/090.
[52] [52] A. Belkind, Z. Zhao, D. Carter, L. Mahoney, G. McDonough, G. Roche, R. Scholl, H. Walde, Pulsed-DC reactive sputtering of dielectrics: pulsing parameter effects, in: 43rd Annual Technical Conference Proceedings, 2000, p. 5.
[53] M. Sridharan, M. Sillassen, J. Bøttiger, J. Chevallier, H. Birkedal, Pulsed DC magnetron sputtered Al2O3 films and their hardness, Surf. Coat. Technol. 202 (2007) 920–924, https://doi.org/10.1016/j.surfcoat.2007.05.061.
[54] J. Sellers, Asymmetric bipolar pulsed DC: the enabling technology for reactive PVD, Surf. Coat. Technol. 98 (1998) 1245–1250, https://doi.org/10.1016/S0257-8972(97)00403-9.
[55] S.V. Fortuna, Y.P. Sharkeev, A.J. Perry, J.N. Matossian, I.A. Shulepov, Microstructural features of wear-resistant titanium nitride coatings deposited by different methods, Thin Solid Films 377–378 (2000) 512–517, https://doi.org/10.1016/S0040-6090(00)01438-3.
[56] T.-S. Yeh, J.-M. Wu, L.-J. Hu, The properties of TiN thin films deposited by pulsed direct current magnetron sputtering, Thin Solid Films 516 (2008) 7294–7298, https://doi.org/10.1016/j.tsf.2008.01.001.
[57] M. Benegra, D.G. Lamas, M.E. Fernández de Rapp, N. Mingolo, A.O. Kunrath, R. M. Souza, Residual stresses in titanium nitride thin films deposited by direct current and pulsed direct current unbalanced magnetron sputtering, Thin Solid Films 494 (2006) 146–150, https://doi.org/10.1016/j.tsf.2005.08.214.
[58] J. Lin, Z.L. Wu, X.H. Zhang, B. Mishra, J.J. Moore, W.D. Sproul, A comparative study of CrNx coatings Synthesized by dc and pulsed dc magnetron sputtering, Thin Solid Films 517 (2009) 1887–1894, https://doi.org/10.1016/j.tsf.2008.09.093.
[59] J.-W. Lee, S.-K. Tien, Y.-C. Kuo, C.-M. Chen, The mechanical properties evaluation of the CrN coatings deposited by the pulsed DC reactive magnetron sputtering, Surf. Coat. Technol. 200 (2006) 3330–3335, https://doi.org/10.1016/j.surfcoat.2005.07.047.
[60] A. Anders, Tutorial: reactive high power impulse magnetron sputtering (R-HiPIMS), J. Appl. Phys. 121 (2017), https://doi.org/10.1063/1.4978350.
[61] H. Elmkhah, F. Attarzadeh, A. Fattah-alhosseini, K.H. Kim, Microstructural and electrochemical comparison between TiN coatings deposited through HIPIMS and DCMS techniques, J. Alloy. Compd. 735 (2018) 422–429, https://doi.org/10.1016/j.jallcom.2017.11.162.
[62] J. Thörnberg, J. Palisaitis, N. Hellgren, F.F. Klimashin, N. Ghafoor, I. Zhirkov, C. Azina, J.-L. Battaglia, A. Kusiak, M.A. Sortica, J.E. Greene, L. Hultman, I. Petrov, P. O.Å. Persson, J. Rosen, Microstructure and materials properties of understoichiometric TiBx thin films grown by HiPIMS, Surf. Coatings Technol. 404 (2020) 126537, doi: 10.1016/j.surfcoat.2020.126537.
[63] K. Zdunek, K. Nowakowska-Langier, J. Dora, R. Chodun, Gas injection as a tool for plasma process control during coating deposition, Surf. Coat. Technol. 228 (2013) S367–S373, https://doi.org/10.1016/j.surfcoat.2012.05.101.
[64] L. Skowronski, K. Zdunek, K. Nowakowska-Langier, R. Chodun, M. Trzcinski, M. Kobierski, M.K. Kustra, A.A. Wachowiak, W. Wachowiak, T. Hiller, A. Grabowski, L. Kurpaska, M.K. Naparty, Characterization of microstructural, mechanical and optical properties of TiO2 layers deposited by GIMS and PMS methods, Surf. Coatings Technol. 282 (2015) 16–23, doi: 10.1016/j.surfcoat.2015.10.004.
[65] D. Bernoulli, U. Müller, M. Schwarzenberger, R. Hauert, R. Spolenak, Magnetron sputter deposited tantalum and tantalum nitride thin films: An analysis of phase, hardness and composition, Thin Solid Films 548 (2013) 157–161, https://doi.org/10.1016/j.tsf.2013.09.055.
[66] H. Kashani, M. Heydarzadeh Sohi, H. Kaypour, Microstructural and physical properties of titanium nitride coatings produced by CVD process, Mater. Sci. Eng. A 286 (2000) 324–330, https://doi.org/10.1016/S0921-5093(00)00744-9.
[67] J.A. Sue, Development of arc evaporation of non-stoichiometric titanium nitride coatings, Surf. Coat. Technol. 61 (1993) 115–120, https://doi.org/10.1016/0257-8972(93)90212-7.
[68] T. Nyberg, S. Berg, U. Helmersson, K. Hartig, Eliminating the hysteresis effect for reactive sputtering processes, Appl. Phys. Lett. 86 (2005), https://doi.org/10.1063/1.1906333.
[69] I. Safi, Recent aspects concerning DC reactive magnetron sputtering of thin films: a review, Surf. Coat. Technol. 127 (2000) 203–218, https://doi.org/10.1016/S0257-8972(00)00566-1.
[70] R.D. Arnell, P.J. Kelly, J.W. Bradley, Recent developments in pulsed magnetron sputtering, Surf. Coat. Technol. 188–189 (2004) 158–163, https://doi.org/10.1016/j.surfcoat.2004.08.010.
[71] S. Schiller, K. Goedicke, J. Reschke, V. Kirchhoff, S. Schneider, F. Milde, Pulsed magnetron sputter technology, Surf. Coat. Technol. 61 (1993) 331–337, https://doi.org/10.1016/0257-8972(93)90248-M.
[72] P.J. Kelly, R.D. Arnell, Development of a novel structure zone model relating to the closed-field unbalanced magnetron sputtering system, J. Vac. Sci. Technol. A 16 (1998) 2858–2869, https://doi.org/10.1116/1.581432.
[73] L.B. Jonsson, T. Nyberg, I. Katardjiev, S. Berg, Frequency response in pulsed DC reactive sputtering processes, Thin Solid Films 365 (2000) 43–48, https://doi.org/10.1016/S0040-6090(99)01116-5.
[74] J.W. Bradley, H. Bäcker, P.J. Kelly, R.D. Arnell, Time-resolved Langmuir probe measurements at the substrate position in a pulsed mid-frequency DC magnetron plasma, Surf. Coat. Technol. 135 (2001) 221–228, https://doi.org/10.1016/S0257-8972(00)00990-7.
[75] I. Petrov, L. Hultman, J.-E. Sundgren, J.E. Greene, Polycrystalline TiN films deposited by reactive bias magnetron sputtering: Effects of ion bombardment on resputtering rates, film composition, and microstructure, J. Vac. Sci. Technol. A 10 (1992) 265–272, https://doi.org/10.1116/1.578074.
[76] K. Müller, Stress and microstructure of sputter-deposited thin films: Molecular dynamics investigations, J. Appl. Phys. 62 (1987) 1796–1799, https://doi.org/10.1063/1.339559.
[77] J.F. Archard, Contact and rubbing of flat surfaces, J. Appl. Phys. 24 (1953) 981–988, https://doi.org/10.1063/1.1721448.
[78] H.G. Howell, J. Mazur, Amontons' law and fibre friction, J. Textile Inst. Trans. 44 (1953) T59–T69, https://doi.org/10.1080/19447025308659728.
[79] F.P. Bowden, D. Tabor, The Friction and Lubrication of Solids, Clarendon Press, 1954.
[80] K. Hokkirigawa, K. Kato, An experimental and theoretical investigation of ploughing, cutting and wedge formation during abrasive wear, Tribol. Int. 21 (1988) 51–57, https://doi.org/10.1016/0301-679X(88)90128-4.
[81] E.O. Hall, The deformation and ageing of mild steel: III Discussion and results, Proc. Phys. Soc. London, Sect. B 64 (1951) 747–753, https://doi.org/10.1088/0370-1301/64/9/303.
[82] N.J. Petch, The cleavage strength of polycrystals, Journal of the Iron and Steel Institute. 174 (1953) 25–28.
[83] N.A. Richter, Y.F. Zhang, D.Y. Xie, R. Su, Q. Li, S. Xue, T. Niu, J. Wang, H. Wang, X. Zhang, Microstructural evolution of nanotwinned Al-Zr alloy with significant 9R phase, Mater. Res. Lett. 9 (2021) 91–98, https://doi.org/10.1080/21663831.2020.1840451.
[84] I. Hacisalihoglu, F. Yildiz, A. Alsaran, Wear performance of different nitride-based coatings on plasma nitrided AISI M2 tool steel in dry and lubricated conditions, Wear 384–385 (2017) 159–168, https://doi.org/10.1016/j.wear.2017.01.117.
[85] A. Bahrami, S.H.M. Anijdan, M.A. Golozar, M. Shamanian, N. Varahram, Effects of conventional heat treatment on wear resistance of AISI H13 tool steel, Wear 258 (2005) 846–851, https://doi.org/10.1016/j.wear.2004.09.008.
[86] S.K. Singh, S. Chattopadhyaya, A. Pramanik, S. Kumar, Wear behavior of chromium nitride coating in dry condition at lower sliding velocity and load, Int. J. Adv. Manuf. Technol. 96 (2018) 1665–1675, https://doi.org/10.1007/s00170-017-0796-x.
[87] N. Yasavol, A. Ramalho, Wear properties of friction stir processed AISI D2 tool steel, Tribol. Int. 91 (2015) 177–183, https://doi.org/10.1016/j.triboint.2015.07.001.
[88] J.A. Sue, T.P. Chang, Friction and wear behavior of titanium nitride, zirconium nitride and chromium nitride coatings at elevated temperatures, Surf. Coat. Technol. 76–77 (1995) 61–69, https://doi.org/10.1016/0257-8972(95)02506-5.

[89] L. Aihua, D. Jianxin, C. Haibing, C. Yangyang, Z. Jun, Friction and wear properties of TiN, TiAlN, AlTiN and CrAlN PVD nitride coatings, Int. J. Refract. Metal. Hard Mater. 31 (2012) 82–88, https://doi.org/10.1016/j.ijrmhm.2011.09.010.
[90] S. Lafaye, C. Gauthier, R. Schirrer, The ploughing friction: analytical model with elastic recovery for a conical tip with a blunted spherical extremity, Tribol. Lett. 21 (2006) 95–99, https://doi.org/10.1007/s11249-006-9018-7.
[91] I. Alabd Alhafez, A. Brodyanski, M. Kopnarski, H.M. Urbassek, Influence of Tip geometry on nanoscratching, Tribol. Lett. 65 (2017) 26, https://doi.org/10.1007/s11249-016-0804-6.